PNAS
www.pnas.org

Supplementary Information for

Viral neutralization by antibody-imposed physical disruption

Qingbing Zheng[a,b,1], Jie Jiang[a,b,1], Maozhou He[a,b,1], Zizheng Zheng[a,b,1], Hai Yu[a,b], Tingting Li[a,b], Wenhui Xue[a,b], Zimin Tang[a,b], Dong Ying [a,b], Zekai Li[a,b], Shuo Song[a,b], Xinlin Liu[a,b], Kaihang Wang[a,b], Zhiqing Zhang[a,b], Daning Wang[a,b], Yingbin Wang[a,b], Xiaodong Yan[b,c], Qinjian Zhao[a,b], Jun Zhang[a,b], Ying Gu[a,b,2], Shaowei Li[a,b,2], Ningshao Xia[a,b,2].

Author Affiliations: [a] State Key Laboratory of Molecular Vaccinology and Molecular Diagnostics, School of Life Sciences, School of Public Health, Xiamen University, Xiamen, China 361102 [b] National Institute of Diagnostics and Vaccine Development in Infectious Disease, Xiamen University, Xiamen, China 361102 [c] Department of Chemistry and Biochemistry, Division of Biological Sciences, University of California, San Diego, La Jolla, CA 92093, USA. [1] These authors contributed equally to this work.

Corresponding author: Ying Gu, Shaowei Li, Ningshao Xia.
Email: guying@xmu.edu.cn (Y.G.); shaowei@xmu.edu.cn (S.L.) or nsxia@xmu.edu.cn (N.X.)

This PDF file includes:

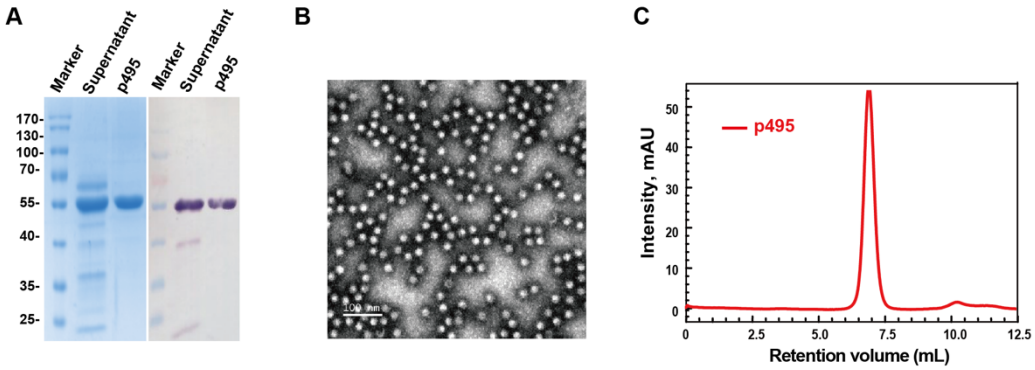

Fig. S1. Characterization of HEV VLPs. (*A*) SDS-PAGE and western blot analysis of the supernatant of insect cell lysates and purified HEV p495 proteins. (***B*)** Negative staining image of purified HEV p495 proteins. The p495 particles assume typical HEV virus-like particles (VLPs). Scale bar is 100 nm. (***C*)** HPSEC profile of purified HEV VLPs.

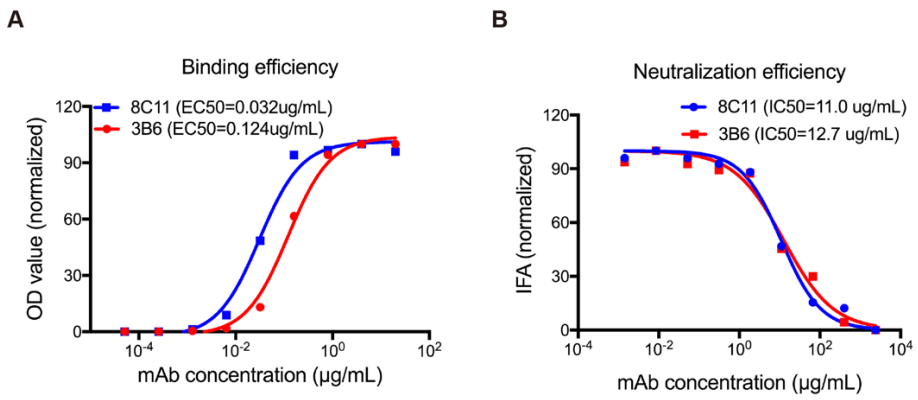

Fig. S2. Binding and neutralizing efficiencies of anti-HEV nAbs 8C11 and 3B6. (*A*) Reactivity of nAbs with E2 protein, as tested by ELISA. The EC50 was calculated using sigmoid trend fitting. **(*B*)** Neutralizing efficiency of nAbs, as tested using a HepG2 cell-infection model. The IC50 was calculated by sigmoid trend fitting.

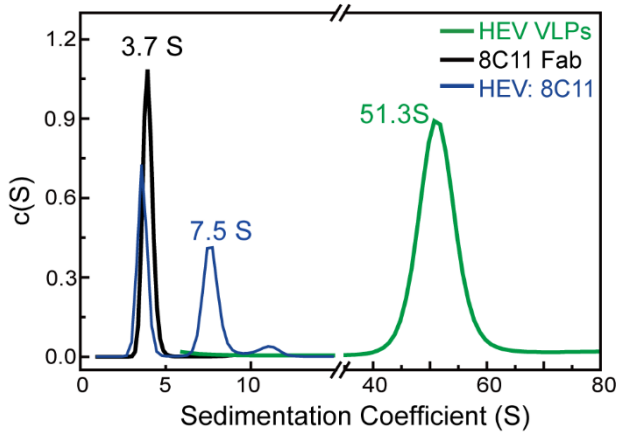

Fig. S3. Sedimentation velocity test of the VLP:8C11 complex. HEV VLPs, Fab 8C11 and VLP:8C11 complex (harvested from the extra peak in question) were subjected to SV tests. c(S) profiles show that the species of the extra peak in question in Figure 1c possesses a sedimentation coefficient (S) larger than 8C11 but much smaller than HEV VLPs.

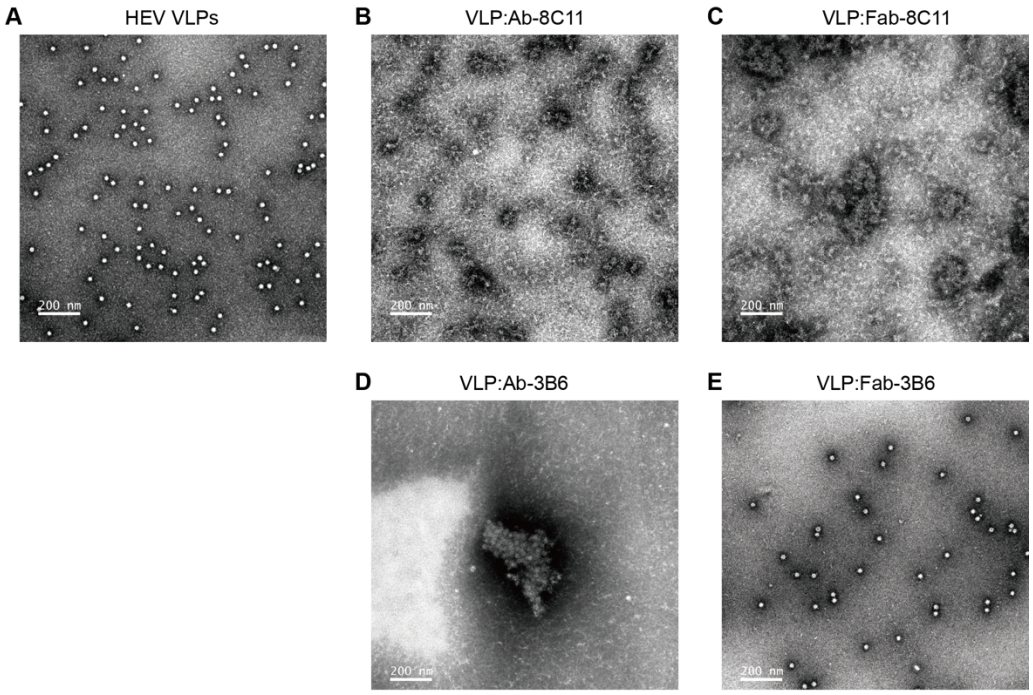

Fig. S4. The dissociation potential of intact antibody of 8C11 observed by negative staining TEM. (*A*) HEV VLPs as control; **(*B* and *C*)** Dissociation of VLPs can be observed when incubating with both intact antibody of 8C11 (*B*) or Fab (*C*). **(*D* and *E*)** Neither intact antibody of 3B6 (*D*) nor its Fab fragment (*E*) was capable to dissociate VLPs.

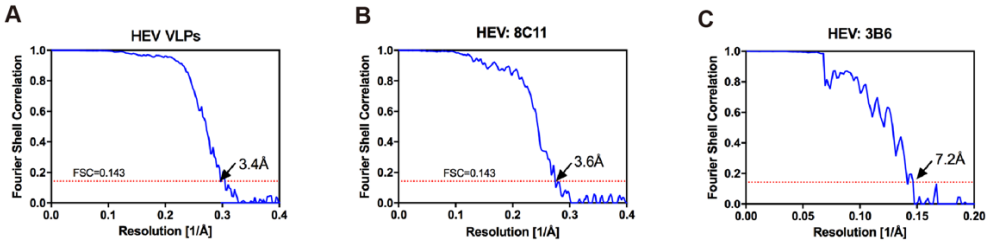

Fig. S5. FSC curves of the 3D reconstructions of HEV VLPs (*A*), VPL:8C11 (*B*) and VLP:3B6 (*C*). Gold-standard Fourier shell correlation (FSC) of reconstructions were plotted against spatial frequency. The resolutions of the three reconstructions were 3.4 Å, 3.6 Å and 7.2 Å, respectively.

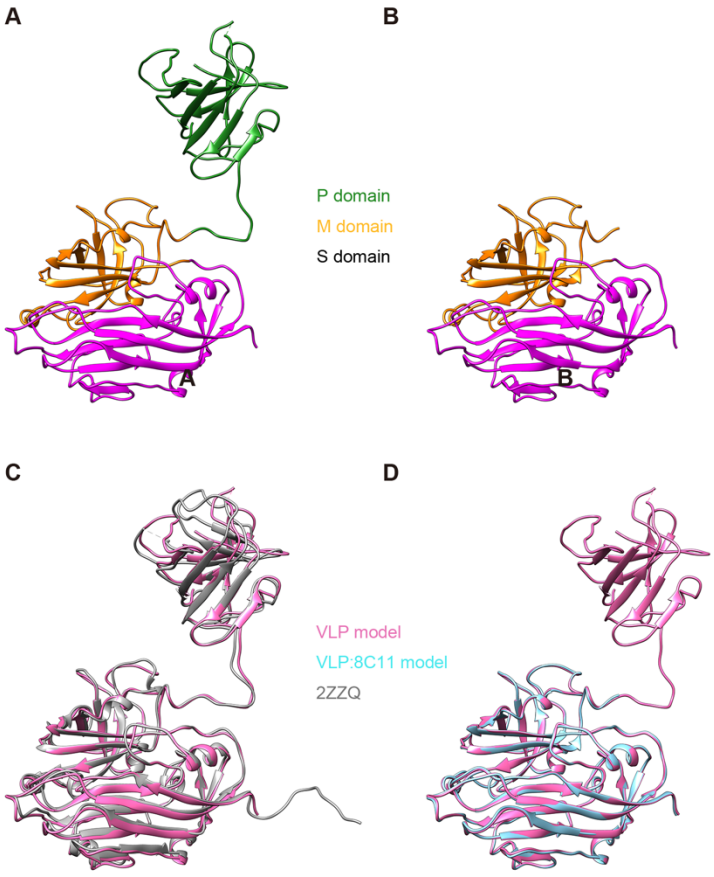

Fig. S6. Structural comparison of p495 monomers from cryo-EM and crystal structures. (*A* and *B*) p495 models built according to cryo-EM density maps of VLP (*A*) and VLP:8C11 (*B*) respectively. P, M, and S domains of p495 are colored in green, orange and magenta, respectively. The models of P domain and 8C11 Fab are not buildable for VLP:8C11 due to little interpretable density. **(*C*)** p495 model of VLP cryo-EM structure is similar to known crystal structure (PDB No. 2ZZQ, an RMSD of 0.90 Å for all aligned Cα atoms). **(*D*)** the models of M and S domains for VLP and VLP:8C11 are quite similar (RMSD=0.29 Å).

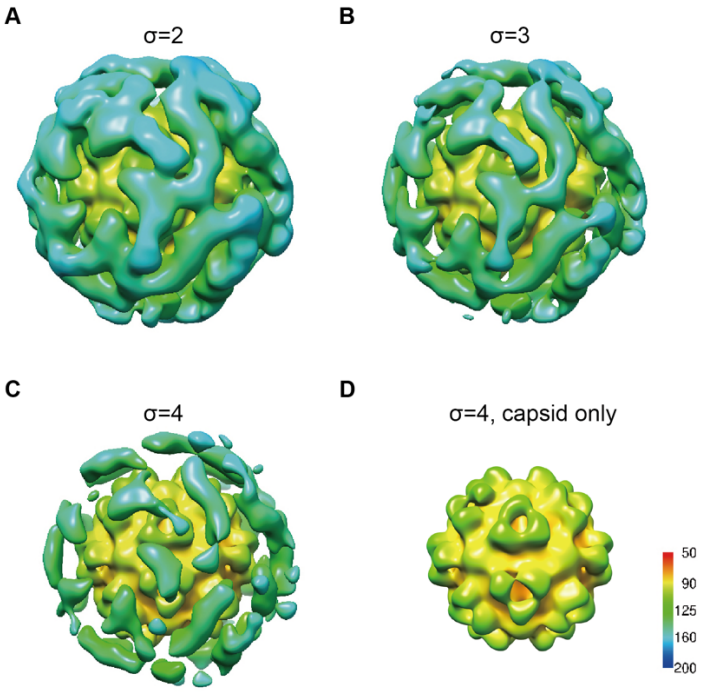

Fig. S7. Cryo-EM reconstruction of the VLP:8C11 complex in asymmetric manner. (*A-C*), Iso-contoured views (colored radially) of cryo-EM maps are displayed at three different contour levels: σ= 3.0 (*A*), σ= 4.0 (*B*) and σ= 5.0 (*C*). **(*D*)** the icosahedral inner shell is conspicuous even under the C1 reconstruction without any symmetry.

Table S1. Statistics of particles selected from VLP:8C11 complexes incubated at different times

	HEV-VLP	VLP:8C11 (15 min)	VLP:8C11 (30 min)	VLP:8C11 (60 min)	VLP:8C11 (2 h)
No. of cryo-EM images	468	227	105	189	122
No. of selected particles	14,269	10,277	2308	893	289
Average particles per image	30	45	22	5	2

Table S2. Statistics of 3D reconstruction and model refinement

	HEV-VLP	HEV: 8C11	HEV: 3B6
Data Collection			
EM equipment		Tecnai F30	
Voltage (kV)		300	
Pixel size (Å)		1.128	
Electron dose ($e^-/Å^2$)		25	
Detector		Falcon II	
Defocus range (μm)	0.9 - 2.8	0.8 - 3.6	1.1 - 3.7
Reconstruction			
Software		Relion 1.4	
Number of used Particles	13,759	4,259	1,029
Final Resolution (Å)	3.4	3.6	7.2
Map sharpening B-factor ($Å^2$)	-188.71	-173.56	-150.00
Model building			
Software	Coot	Coot	/
Refinement			
Software	Phenix	Phenix	/
Model statistics			
Correlation coefficient (around atoms)	0.85	0.87	/
No. of atoms of protein	3,484	2,469	/
Ramachandran outliers	0.00%	0.00%	/
Ramachandran favored	92.04%	93.48%	/
Rotamer outliers	0.79%	0.00%	/
C-beta deviations	0	0	/
Clash score	4.04	3.87	/
RMS(bonds)	0.0118	0.0068	/
RMS(angles)	1.38	1.13	/